2000 IEEE MTT-S Int. Microwave Symp. Dig., Boston, MA, June 12-16, 2000, pp. 1473-1476. Presented by Kate Remley.

TH2C-5

REALISTIC SAMPLING-CIRCUIT MODEL FOR A NOSE-TO-NOSE SIMULATION[1]

Kate A. Remley, Dylan F. Williams, and Donald C. DeGroot
National Institute of Standards and Technology
RF Electronics Group
325 Broadway
Boulder, CO 80303-3328

***Abstract* – We extend previously developed oscilloscope sampler models to include realistic circuit characteristics and use these models to investigate the nose-to-nose calibration technique.**

INTRODUCTION

We extend the SPICE model for a broadband sampling circuit that we developed in [1] and use this model to find the overall response of the circuit. We then investigate how circuit nonidealities affect the accuracy of the nose-to-nose calibration [2], which estimates the forward transfer function of the sampler.

The original analytic development of the nose-to-nose calibration procedure [3-5] simplified the treatment of the strobe-generator impedance, strobe-shaping network, nonlinear diode capacitance, and diode imbalance. In [1] we developed a SPICE model of a broadband sampling circuit [6] that can be used to study the effects of such nonidealities and verified the simulation technique. Here we extend our circuit model to include these nonideal effects and show how they influence errors in the nose-to-nose calibration.

ESTIMATE OF THE FORWARD TRANSFER FUNCTION

The nose-to-nose calibration [2-5] provides an estimate of the forward transfer function of a broadband sampling oscilloscope; the estimate can then be used to correct measurements made with the oscilloscope. The premise of the nose-to-nose calibration is that the sampler kickout, which is generated at the input port of a two-diode sampling circuit (see Fig. 1) when a DC offset is applied to the diode bias, is proportional to the sampler's forward transfer function [2].

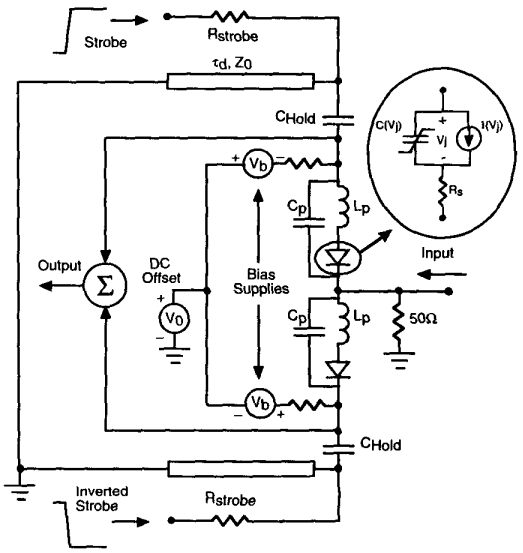

Fig. 1. Simplified schematic of the sampling circuit. The inset shows the large-signal equivalent circuit of the diode.

In a nose-to-nose calibration, the input ports of two impedance-matched samplers, which we will call A and B, are connected directly together (nose-to-nose). References [3-5] show that, in the absence of reflections or mismatches, the response of the entire system is proportional to the convolution of the time-domain representation of the forward transfer function (called the impulse response in [1-5]) of sampler A and the kickout of sampler B. In the frequency domain we have

$$M(\omega)_{AB} \cong K_B(\omega)H_A(\omega), \qquad (1)$$

where M_{AB} is the measured waveform, H_A is the forward transfer function of sampler A and

[1] Publication of the National Institute of Standards and Technology, not subject to copyright

K_B is the Fourier transform of the kickout pulse emanating from sampler B. An estimate of the forward transfer function of sampler A can be found from a set of three measurements of three samplers [5],

$$H_A(\omega)^{est} \equiv C\sqrt{\frac{M_{AB}(\omega)M_{AC}(\omega)}{M_{BC}(\omega)}}$$

$$\cong CH_A(\omega)\sqrt{\frac{K_B(\omega)}{H_B(\omega)}}, \qquad (2)$$

where C is a simple proportionality constant.

We define the error ratio E of the sampler response estimate as

$$E(\omega) \equiv \frac{H_A{}^{est}(\omega)}{H_A(\omega)} \cong C\sqrt{\frac{K_B(\omega)}{H_B(\omega)}}, \qquad (3)$$

where we chose C such that $E(0)=1$. Equation (3) states that the error ratio E in the nose-to-nose calibration procedure (assuming linearity, ideal connection networks, and a perfect oscilloscope timebase) can be approximated as the square root of the Fourier transform of the kickout function divided by the sampler's forward transfer function. The closer the shapes of the kickout function and the forward transfer function, the smaller the error ratio and the more accurate the calibration.

In the present work, we use a SPICE model to simulate the broadband sampler described in [6], but with a strobe pulse of shorter duration to more closely approximate modern samplers. We use the SPICE simulations to determine $K(\omega)$ and $H(\omega)$, improving numerical accuracy compared with determining M directly. Convergence studies of our SPICE models indicate that our resolution is about 0.03dB in magnitude and 0.05 degrees in phase for calculations of the error ratio E. In the following we examine noncorrectable nose-to-nose calibration errors related to three factors: strobe pulse-generator impedance, nonlinear diode junction capacitance, and diode imbalance.

STROBE-GENERATOR IMPEDANCE AND PULSE-SHAPING CIRCUITRY

The strobe pulse forward biases the sampling diodes during a brief sampling interval, allowing current to flow from the input port through the hold capacitors. Ideally, the differential charge stored on the hold capacitors during the sampling interval is proportional to the input signal at the time the sample is taken.

In the original nose-to-nose analyses [3-5], and in our earlier work [1], the strobe generator was modeled as an ideal pulse source, with source impedance of 0 Ω. However, the sampler described in [6] uses a step generator with source impedance of approximately 57 Ω that drives an 85.2 Ω transmission line shorted at its far end. The voltage step initially turns the diode on, while the reflection of the step from the end of the transmission line turns the diode off at $2\tau_d$, where τ_d is the transmission line delay (see Fig. 1). In this experiment, the rise time of the pulse was 10 ps and τ_d was 7 ps, and we used a two-section ladder network to implement the transmission line in SPICE.

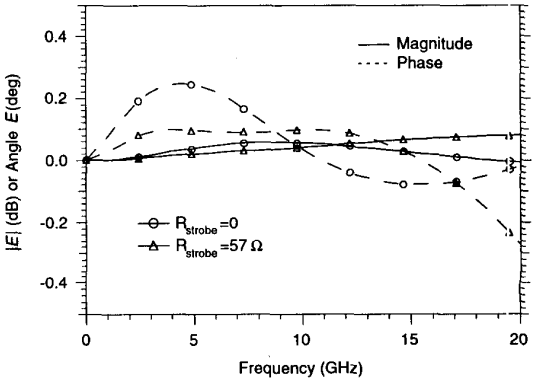

Fig. 2. The error ratio E from (3) for an ideal, zero-impedance strobe generator and for one with 57 Ω impedance and transmission line pulse shaping.

Figure 2 shows simulation results of the error ratio E as defined in (3) for the sampler with pulse-shaping circuitry compared to the error ratio for a sampler having 0 Ω strobe-generator impedance. The zero-impedance strobe pulse was formed using an ideal source in SPICE with comparable pulse duration. The results show that the error ratio is minimally affected by the finite strobe-generator impedance and, for certain frequencies, the error is less.

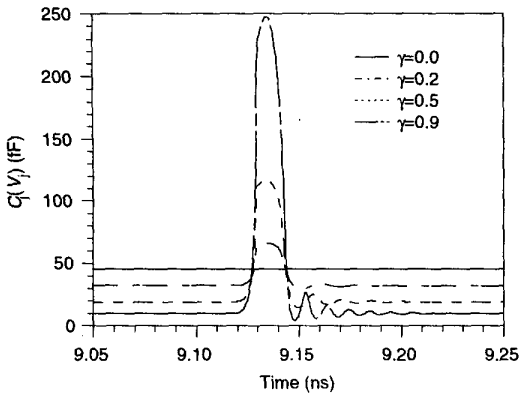

Fig. 3. Junction capacitance $C(V_j)$ for various values of grading coefficient, γ. The spreading resistance R_s is 19 Ω, the zero-bias junction capacitance C_{j0} is 0.045 pF, the saturation current I_s is 26.7 pA, the emission coefficient N is 1.08, the activation energy E_G is 0.69 eV, the built-in junction potential ϕ_{bi} is 0.7 V, and the minority carrier transit time τ_t is zero. The strobe generator impedance is 57 Ω and utilizes transmission line pulse shaping.

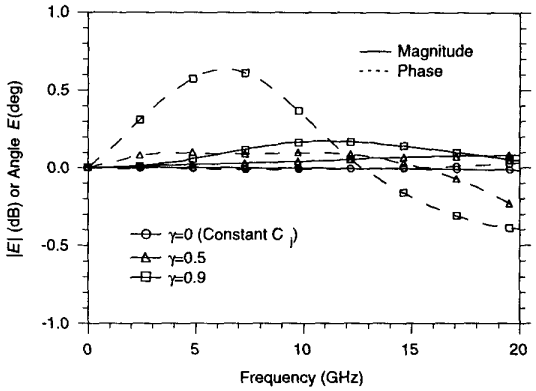

Fig. 4. Error ratio E for various values of grading coefficient γ. τ_t is set to zero and the other diode parameters are given in the caption of Fig. 3.

NONLINEAR DIODE CAPACITANCE

In the original analyses of the nose-to-nose calibration [3-5], the diode junction capacitance was fixed and did not depend on the junction voltage V_j. Because SPICE provides a full diode model, we are able to include the effects of the voltage-dependent diode capacitance in the simulation.

The diode model used in SPICE [7] is shown in the inset of Fig. 1. The diode junction is represented as a voltage-controlled current source in parallel with a nonlinear capacitance. The junction is in series with a parasitic spreading resistance R_s, which is treated as a linear quantity.

SPICE can incorporate two types of nonlinear diode capacitance. The first is the junction capacitance

$$C_j(V_j) = \frac{C_{j0}}{\left(1 - \frac{V_j(t)}{\phi_{bi}}\right)^{\gamma}}, \qquad (5)$$

where C_{j0} is the zero-voltage junction capacitance, ϕ_{bi} is the junction's built-in potential, and γ is the grading coefficient. The second type of nonlinear capacitance incorporated in SPICE diode models is $C_D(V_j)$, the diffusion capacitance. This capacitance is associated with the minority carrier transit time τ_t, and is given by

$$C_D(V_j) = \tau_t \, g_d(V_j), \qquad (6)$$

where $g_d(V_j) = dI(V_j)/dV_j$ is the small-signal junction conductance.

Figure 3 shows the time-varying junction capacitance from our simulations for various values of diode grading coefficient γ. The junction capacitance is constant and equal to C_{j0} when γ = 0, and the doping of the epitaxial layer is linearly graded when γ = 0.5. Note that the larger the grading coefficient, the larger the change in $C_j(V_j)$ with time.

Figure 4 indicates that the error ratio E in the nose-to-nose calibration is smallest in both phase and amplitude when the junction capacitance is constant, and the error increases for increasing nonlinear capacitance $C_j(V_j)$. Nevertheless, the simulation results indicate that the magnitude error is less than 0.1 dB and the phase error less than 0.3 degrees up to 20 GHz for a linearly-graded diode junction (γ = 0.5), typical for a Schottky-barrier diode.

Figure 5 shows that minority carrier transit time, which increases nonlinear capacitance in the diode, increases the error ratio E significantly above our 0.03 dB/0.05 degree resolution limit. Because many samplers use Schottky-barrier diodes, in practice the diffusion capacitance is usually negligible due to the absence of minority carriers [7].

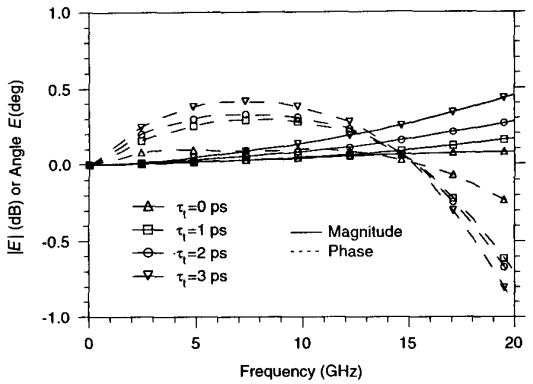

Fig. 5. Error ratio in the nose-to-nose calibration for various minority carrier transit times τ_l. The grading coefficient γ is 0.5. Other parameters are given in the caption of Fig. 3. In [1], τ_l =3 ps.

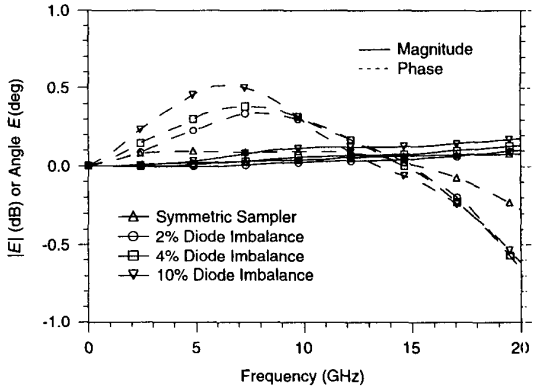

Fig. 6. Estimate of the error ratio with diode imbalance. The grading coefficient γ is 0.5, τ_l is zero, and the other diode parameters are given in the caption of Fig. 3.

DIODE IMBALANCE

The balanced design of the two-diode sampler of Fig. 1 ensures that differential charges transferred by the strobe pulse to the hold capacitors cancel at the sampler input port and at the output amplifier. However, if the two diodes are not identical, the strobe will leave a residual charge on the hold capacitors which results in a DC offset at the output amplifier. In addition, some of the strobe pulse will "leak" through to the sampler input port. In practice, one performs two nose-to-nose measurements, one with a positive bias offset (V_0 Fig. 1) and one with a negative bias offset in an attempt to eliminate the common-mode leakage at the input port [4, 5]. The DC offset at the output port must be subtracted before nose-to-nose measurements are conducted.

Figure 6 shows simulation results in which we deliberately introduced diode imbalance into the sampling circuit by increasing the area parameter for one diode junction while decreasing the area parameter of the other. With a 4 % diode imbalance, the common-mode leakage was only about 5 % of the kickout pulse in amplitude. This fact, combined with the subtraction process described above, may help to explain the minimal degradation of the sampler circuit response estimate.

CONCLUSION

We used a SPICE model for a broadband sampling circuit to evaluate some of the non-correctable errors in the nose-to-nose calibration technique. The model showed that strobe-generator impedance and pulse-shaping circuitry have a minor effect on the error. Nonlinear diode capacitance and, to a lesser extent, diode imbalance may increase the nose-to-nose error. However, in the many of the cases we studied the error remains small over a wide range of parameter values.

REFERENCES

[1] D. F. Williams, K. A. Remley, and D. C. DeGroot, "Nose-to-nose response of a 20-GHz sampling circuit," in *54th ARFTG Conference Digest*, Atlanta, GA, Dec. 2-3 1999, pp. 64-70.

[2] K. Rush, S. Draving, and J. Kerley, "Characterizing high-speed oscilloscopes," *IEEE Spectrum*, no. 9, pp. 38-39, Sept. 1990.

[3] J. Verspecht and K. Rush, "Individual characterization of broadband sampling oscilloscopes with a nose-to-nose calibration procedure," *IEEE Trans. Instrum. Meas.*, vol. 43, no. 2, pp. 347-354, Apr. 1994.

[4] J. Verspecht, "Calibration of a Measurement System for High Frequency Nonlinear Devices," Ch. 4, Ph. D. Thesis, Free University of Brussels, Brussels, Belgium, Sept. 1995.

[5] J. Verspecht, "Broadband sampling oscilloscope characterization with the 'nose-to-nose' calibration procedure: a theoretical and practical analysis," *IEEE Trans. Instrum. Meas.*, vol. 44, no. 6, pp. 991-997, Dec. 1995.

[6] S. Riad, "Modeling of the HP-1430A feedthrough wideband (28-ps) sampling head," *IEEE Trans. Instrum. Meas.*, vol. IM-31, no. 6, pp. 110-115, June 1982.

[7] A. Vladimirescu, *The SPICE Book*. New York: Wiley and Sons, 1994.